JOURNAL OF PROPULSION AND POWER
Vol. 16, No. 2, March–April 2000

Feasibility Assessment of Thermal Barriers for Extreme Transient Temperatures

Bruce M. Steinetz*
NASA John H. Glenn Research Center at Lewis Field, Cleveland, Ohio 44135
and
Patrick H. Dunlap Jr.†
Modern Technologies Corporation, Middleburg Heights, Ohio 44130

Assembly joints of modern solid rocket motor cases are generally sealed using conventional O-ring seals. The 5500°F combustion gases produced by rocket motors are kept a safe distance away from the seals by thick layers of phenolic insulation. Special compounds are used to fill insulation gaps leading up to the seals to prevent a direct flowpath to them. Design criteria require that the seals should not experience torching or charring during operation, or their sealing ability would be compromised. On limited occasions, NASA has observed charring of the primary O-rings of the space shuttle solid rocket nozzle assembly joints because of parasitic leakage paths opening up in the gap-fill compounds during rocket operation. NASA is investigating different approaches for preventing torching or charring of the primary O-rings. One approach is to implement a braided rope upstream of the primary O-ring to serve as a thermal barrier that prevents the hot gases from impinging on the O-ring seals. This paper presents flow, resiliency, and thermal resistance for several types of NASA thermal barriers braided out of carbon fibers. Burn tests were performed to determine the time to burn through each of the thermal barriers when exposed to the flame of an oxyacetylene torch (5500°F), representative of the 5500°F solid rocket motor combustion temperatures. Thermal barriers braided out of carbon fibers endured the flame for over six minutes, three times longer than the solid rocket motor burn time. Room and high temperature flow tests are presented for the thermal barriers for different amounts of linear compression. Room temperature compression tests were performed to assess resiliency and unit preloads as a function of compression. The thermal barrier was tested in a subscale rocket char motor test in which it served to impede hot gas flow through an intentionally oversized defect in the gap insulation. Temperature measurements indicated a 2200°F temperature drop across the $\frac{1}{4}$-in.-diam thermal barrier with no apparent signs of burning or charring.

Introduction

THE need for high temperature (1500–2000°F) compliant seals in increasingly demanding gas turbine engine designs led to the development of rope seals braided out of emerging ceramic fibers and superalloy wires. Previous seal research yielded several braided rope seal designs that demonstrated the ability to both seal and serve as compliant mounts under aggressive temperature and pressure requirements.[1,2] These seals have low leakage, exhibit resilience with cycling to maintain a good seal, resist scrubbing damage, seal complex geometries, and support structural loads. Steinetz et al.[1] and Steinetz and Adams[2] studied both all-ceramic and hybrid designs that were applied in industrial tube seal and high or low pressure turbine vane seal applications. The material systems used in these braided rope seal designs function very well at the temperatures experienced in advanced gas turbine engines. However, as revealed later in this study, these seals do not last for more than a few seconds when subjected to the extremely hot 5500°F combustion gases that are found in rocket applications. Thus, other materials had to be considered to advance the braided rope seal design into a thermal barrier for use at extreme transient temperatures.

Solid rockets, including the space shuttle reusable solid rocket motor (RSRM), have assembly joints that are usually sealed by conventional O-ring type seals. These seals are shielded from the 5500°F combustion gases by thick layers of phenolic insulation and by special compounds that fill gaps in this insulation. Normally, these two stages of protection are enough to prevent a direct flow of the 900 psi hot gases to the seals. Occasionally, though, seals have experienced charring because of parasitic leakage paths that open up in the gap-filling compounds during rocket operation, requiring another level of protection for the primary O-rings. Inspection during disassembly of space shuttle solid rocket motor nozzle joints from RSRM-44 and RSRM-45 revealed O-ring erosion of joint 3 primary O-ring seals[3] (Fig. 1a). NASA and rocket manufacturer Thiokol are investigating nozzle joint design enhancements, such as the proposed thermal barrier (Figs. 1a and 1b), to prevent hot combustion gases from reaching the Viton primary O-rings. The nozzle-to-case joint and joints 1 through 5 in Fig. 1 are currently being studied. The braided carbon thermal barrier being developed at NASA Glenn is a leading candidate based on the results presented herein. The thermal barrier has unique requirements for the shuttle solid rocket motor joints, including the following: 1) sustain extreme temperatures (2500–5500°F) during solid rocket motor burn (2 min and 4 s) without loss of integrity, 2) block 900 psi hot flow gases from impinging on primary O-rings to prevent O-ring char or erosion, 3) exhibit some permeability to allow pressure check of primary/secondary O-ring system without any false-positives of the primary O-ring seal, and 4) exhibit adequate resiliency/springback to accommodate limited (0.003–0.005 in.) joint movement/separation and to seal manufacturing tolerances in these large nozzle segments (diameter range: 4.8–7.3 ft).

Over the past few decades, carbon fibers have been used in a wide variety of applications in aerospace because of their excellent combination of thermal and mechanical properties. Among heat-resistant fibers, carbon fibers have been widely used because of their relatively high heat conduction, low linear expansion coefficient, and high corrosion and thermal stability as well as their high strength

Received 15 August 1998; revision received 3 April 1999; accepted for publication 16 April 1999.

*Senior Research Engineer, Mechanical Components Branch. Member AIAA.

†Research Engineer, 7530 Lucerne Drive, Islander Two, Suite 206, Middleburg Heights, OH 44130.

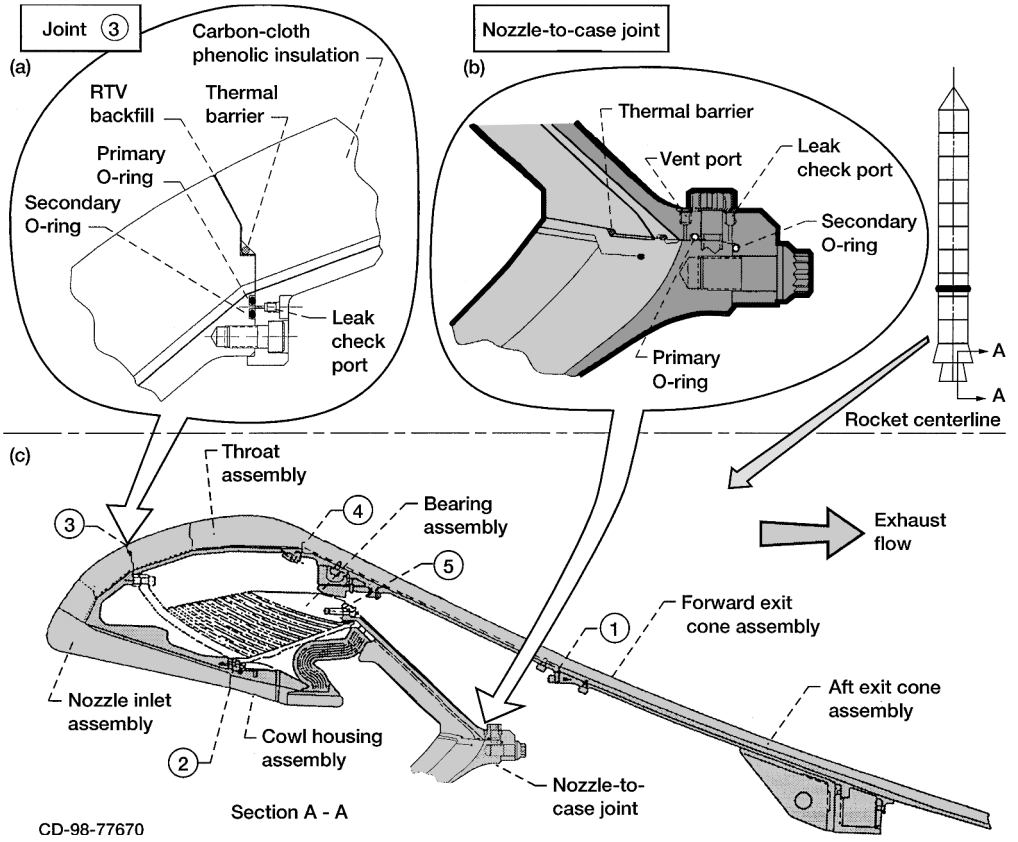

Fig. 1 Potential shuttle solid rocket motor joint locations for candidate thermal barrier. Enlarged view of a) Joint 3 and b) nozzle-to-case joint showing primary and secondary pressure O-rings, leak-check port, and proposed thermal barrier location. c) Overall nozzle cross section (half view).

and low density.[4] Though braided carbon thermal barriers have been used for nuclear applications, there are no known uses of this type of thermal barrier for solid rocket applications. Although carbon fibers oxidize and lose mass over periods of several hours at temperatures above 600–900°F (depending on the type of fiber),[5–7] they are able to withstand very high temperatures for short periods of time.

The main objective of the current study was to evaluate the thermal resistance of braided rope thermal barriers made of different materials, including carbon, when exposed to extremely high-temperature gases. The thermal barriers that endured these gases the longest were then subjected to flow and compression tests. Subscale rocket char motor tests were performed to assess the thermal barrier's heat resistance under actual rocket conditions.

Test Apparatus and Procedures

Thermal Barrier Specimens

Several types of thermal barriers were examined for each different series of tests. Carbon, phenolic, hybrid, and all-ceramic braided rope seals and thermal barriers were all subjected to burn tests. Buna-N and Viton rubber seals and a $\frac{1}{8}$-in.-diam stainless steel rod were also burn tested as references to compare to the braided rope materials. Table 1 summarizes the relevant architecture parameters for the braided rope thermal barriers that were tested. All thermal barriers were composed of a dense uniaxial core of fibers overbraided with a single- or multi-layer sheath.

The Carbon-1 design had five sheath layers and a 0.114-in. diam, whereas Carbon-2 had ten sheath layers and a 0.125-in. diam. Both the Carbon-3 and Carbon-4 designs had five sheath layers. However, Carbon-3 had a 0.200-in. diam, and Carbon-4 had a 0.194-in. diam. Carbon-4 had 4.4×10^{-4}-in. (11 μm) pitch-based Amoco P25 fibers in their cores to evaluate core fiber diameter effects on performance, whereas the core fibers of all of the other carbon thermal barriers were 2.76×10^{-4}-in. (6.9 μm) PAN (polyacrylonitrile)-based Grafil-type 34-700 fibers. PAN-based Thornel T-300 carbon fibers with a 2.8×10^{-4}-in. (7 μm) diameter were used in the sheaths of all of the carbon thermal barriers. The phenolic design had a core composed of Kynol KFY-0204-1 fibers with diameters of 6.0×10^{-4} in. (15 μm) and a four-layer sheath of 6.0×10^{-4}-in. (15 μm) Kynol KY-02 fibers. Hybrid and all-ceramic braided construction details are presented in Table 1.

Thermal Barrier Characterization

To assess thermal barrier architecture characteristics, samples of each carbon fiber braided thermal barrier design were examined using a photographic stereomicroscope. Two cross-sections of each type of thermal barrier about $\frac{1}{16}$-in. thick were prepared and examined under the microscope. Photographs were taken of each side of the specimen at 30X for the 0.20-in.-diam thermal barriers or 40X for the $\frac{1}{8}$-in.-diam designs, so that four cross section photos were examined for each type of thermal barrier. None of the core areas were completely round, so the dimensions of the core were measured using vernier calipers. These dimensions were then used to calculate the area of the core in the cross section. For each area, an equivalent core diameter was calculated as if the core was circular. The core diameters were then used along with the overall thermal barrier diameter for each design to calculate the sheath thickness using the following relationship:

$$\text{Overall diameter} = \text{Core diameter} + 2(\text{Sheath thickness})$$

These values were then averaged from the four photographs to obtain an equivalent core diameter and sheath thickness for each type of carbon thermal barrier.

Overall thermal barrier density measurements were also made for each design. Three 4-in. specimens of each type of thermal barrier were prepared and weighed using a precision electronic balance. The length and diameter of each specimen were measured using vernier calipers. The overall density of each specimen was then calculated by dividing the weight of the specimen by its volume. The

Table 1 Thermal barrier construction matrix

		Core				Sheath						
Barrier type	Size: diameter, in.	Material	Denier	Fiber diameter, in.[a]	Number of yarns	Material	Denier	Fiber diameter, in.[a]	Number of layers	Number of carriers per layer	Number of yarns per bundle	Braid angle, deg
						Carbon						
Carbon-1	0.114	Grafil[b]				Thornel[c]						
		34-700 12k	7200	2.76×10^{-4}	4	T-300 1K	600	2.8×10^{-4}	5	8	1	45
Carbon-2	0.125	Grafil				Thornel						
		34-700 12K	7200	2.76×10^{-4}	1	T-300 1K	600	2.8×10^{-4}	10	8	1	45
		34-700 3K	1800		1							
Carbon-2A	0.125	Grafil				Thornel						
		34-700 12K	7200	2.76×10^{-4}	1	T-300 1K	600	2.8×10^{-4}	9	8	1	45
		34-700 3K	1800		1							
Carbon-3	0.200	Grafil				Thornel				12, 12,		65 in 1st
		34-700 12K	7200	2.76×10^{-4}	10	T-300 1K	600	2.8×10^{-4}	5	24, 24, 24	1	60 in 5th
Carbon-4	0.194	Amoco[d]				Thornel				12, 12		65 in 1st
		P25 2K	2900	4.4×10^{-4}	21	T-300 1K	600	2.8×10^{-4}	5	24, 24, 24	1	60 in 5th
						Phenolic						
Phenolic-1	0.125	Kynol[e]				Kynol						
		KFY-0204-1	4500	6.0×10^{-4}	4	KY-02	1100	6.0×10^{-4}	4	8	1	45
						Hybrid						
NTWHY-4	0.120	NX 550[f]	700	3.2×10^{-4}	154	HS 188[g]	110	1.6×10^{-3}	1	24	6	65
						All-ceramic						
NTWAC-2	0.120	NX 550	700	3.2×10^{-4}	109	NX 550	700	3.2×10^{-4}	2	8	1	56

[a] 1×10^{-3} in. = 25 μm.
[b] Grafil type 34-700 carbon fibers, Grafil Inc. product.
[c] Thornel T-300 carbon fibers, Amoco Performance Products, Inc. product.
[d] Amoco P25 pitch fibers, Amoco Performance Products, Inc. product.
[e] Kynol fibers, American Kynol, Inc. product, 76% C, 18% O, 6% H.
[f] NX 550 = Nextel 550 fiber, 3M product, 73% Al_2O_3, 27% SiO_2.
[g] HS 188 = Haynes 188 wire, Fort Wayne Metals product, 38% Co. 22% Ni, 22% Cr, 14% W, 3% Fe, 1.25% Mn, 0.5% Si, 0.08% La, 0.015% B, 0.05% C.

overall density of each type of thermal barrier was then calculated by averaging the values obtained from the three specimens.

Burn Tests

A simple screening test was developed to evaluate thermal barrier burn resistance under simulated rocket motor combustion temperatures (5500°F) by aiming a neutral flame of an oxyacetylene welding torch at the center section of a 4-in. specimen. In these tests, the amount of time required to cut completely through the specimen was measured. Time for cut-through was measured from the instant the flame touched the specimen until the specimen was completely cut into two separate pieces. These tests were performed using two different setups. The first setup mainly screened different types of thermal barrier materials. One end of the 4-in. sample was held in a clamp, and the remainder of the specimen hung vertically below the clamp. The oxyacetylene torch was adjusted to a neutral flame, and the flame was manually applied to the center section of the thermal barrier with the nozzle exit about one inch away from the specimen. The time to burn through the specimen was recorded from the instant the flame hit the thermal barrier until it was completely cut in half and the lower half fell to the floor. Several different materials were tested including: all-ceramic, hybrid, phenolic, and carbon thermal barriers. All specimens had $\frac{1}{8}$-in. diam. Rubber O-rings made of Buna-N and Viton, and a $\frac{1}{8}$-in.-diam stainless steel rod were also tested for comparison purposes. This method was not well controlled as the application of the flame to the specimen was subject to the torch operator's ability to hold the torch steady and in the same position from test to test. Thus, a more repeatable, consistent method of performing these tests was designed.

In this second approach, two specimens, the test specimen and a flame calibration specimen, were clamped in place in the fixture, so that the surface closest to the torch was 0.30 in. (7.5 mm) from the stationary nozzle (Fig. 2). The carriage that held the clamps was capable of sliding along a machined groove so that either specimen could be positioned in front of the oxyacetylene torch at the same prescribed distance. The torch was placed in between the two specimens and ignited. The first time that the torch was lit for a given series of tests a neutral flame[8] was formed by adjusting the valves on the torch handle. The flame calibration specimen was then slid into the flame to check that the tip of the inner cone of the flame (the hottest part of the flame)[8] was 0.08 in. (2 mm) from the edge of the specimens. Theoretical calculations based on the chemical reactions that occur as the flame burns estimate the temperature at the tip of the inner cone to be about 5500°F (Ref. 9). The test specimen was then slid into the flame, and the amount of time to burn through it was recorded. End-stop clamps were positioned on the fixture at either end of the groove to position the specimens directly in the center of the flame as the carriage moved from one end of the groove to the other. Between tests the gas supply was shut off at the bottles so as not to disturb the sensitive oxygen/acetylene mixture that was regulated at the torch. This ensured that the same mix of oxygen and acetylene was used to burn through each specimen and that the flame was consistent from test to test. After a burned test specimen was removed from the fixture, a new specimen was clamped in place 0.30 in. from the nozzle, and the torch was relit between the specimens. Because the valves on the torch had already been adjusted for a neutral flame, no additional adjustments were needed. However, the position of the flame was always verified using the flame calibration specimen before sliding the test specimen into the flame. Specimens of all four carbon fiber thermal barrier designs were tested using this fixture. The Carbon-1 and Carbon-2 designs had nominal diameters of $\frac{1}{8}$ in., whereas Carbon-3 and Carbon-4 had nominal 0.20-in. diam. An additional design was also tested in which the last sheath layer was removed from a Carbon-2 specimen. This design only had nine sheath layers and was referred to as Carbon-2A.

Flow Tests

Flow tests were performed on the thermal barriers in a high temperature flow and durability test rig shown schematically in Fig. 3. Specimen length was 8.00 ± 0.05 in., and the thermal barriers were mounted into a groove in the piston. The free ends of the specimens were joined together in the piston groove using a $\frac{1}{4}$-in. lap joint. Preload was applied to the specimens through a known interference

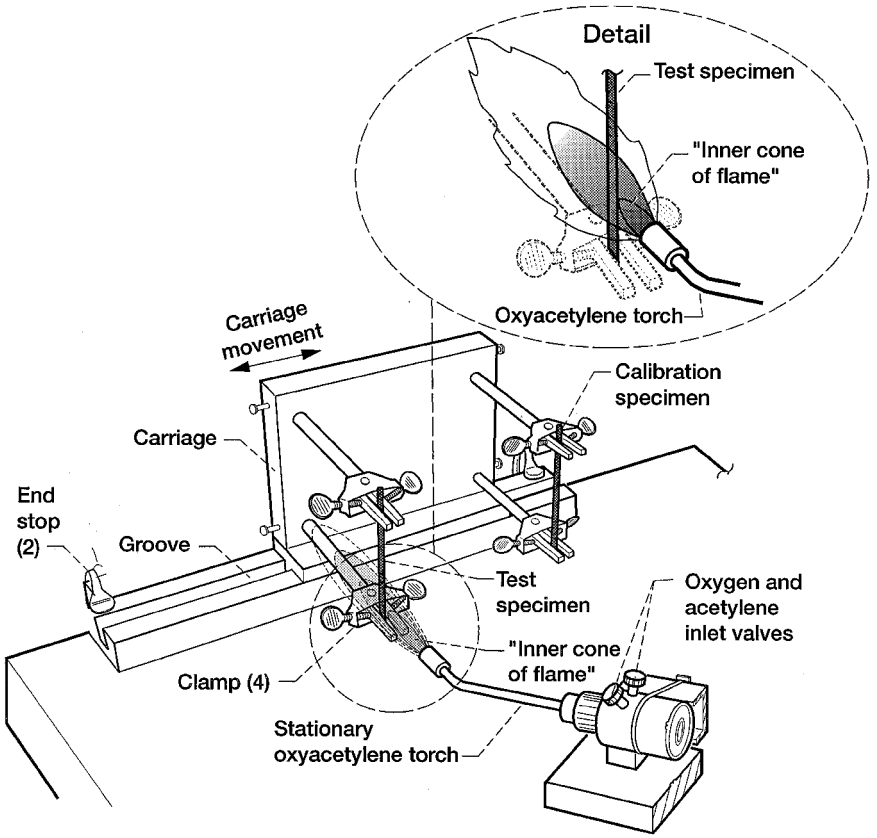

Fig. 2 Schematic of burn test fixture.

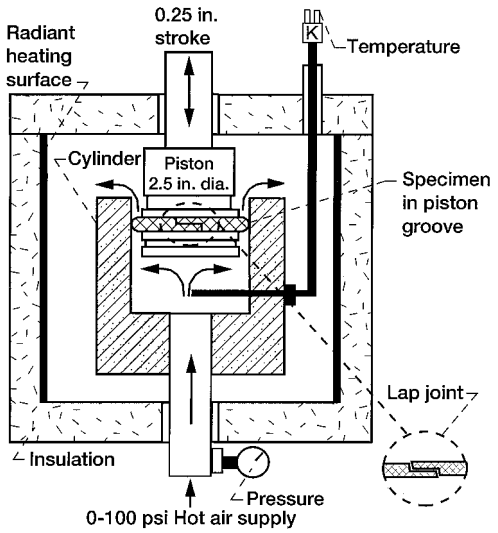

Fig. 3 Schematic of flow fixture.

fit between the thermal barrier and the cylinder inner diameter. To vary the amount of preload, the interference fit was modified by mounting different thicknesses of stainless steel shims behind the specimen in the piston groove. Before flow testing, specimens were preworked or precompressed to minimize damage to them during the process of inserting the piston/thermal barrier assembly into the cylinder. Details of the preworking procedure are described in depth by Steinetz and Adams.[2] After being preworked, the piston/thermal barrier assembly was inserted into the cylinder for testing. During flow testing, hot pressurized air entered at the base of the cylinder and flowed to the test specimen that sealed the annulus created by the cylinder and piston walls. A radial gap of 0.007 in. between the piston and the cylinder created this annulus. The durability of the thermal barriers at high temperatures was examined by subjecting them to scrub cycles in which the piston and thermal barrier were reciprocated in the cylinder. This movement simulated relative thermal growths between structures that the thermal barriers would be sealing. Movement of the piston within the cylinder was guided by preloaded precision linear bearings. The piston stroke for each cycle was 0.125 in., so for each cycle the seal sliding distance was 0.25 in.

The test rig is capable of operating at temperatures from room temperature to 1500°F, pressures between 0 and 100 psig, and flows of 0–3.5 SCFM (standard cubic feet per minute conversion 1 SCFM = 28.3 standard liters per minute). Other details of the high temperature flow and durability test rig including hardware, heating systems, measurement techniques and probe accuracy have been previously described in depth by Steinetz et al.[1] Flow data were recorded before scrubbing at temperatures of 70 and 500°F and after scrubbing at 70, 500, and 900°F. Specimens were subjected to 10 scrub cycles at 500°F. No prescrubbing flow data were collected at 900°F to minimize the amount of carbon fiber oxidation that occurred while the thermal barrier sat at that temperature during rig heat up. At each temperature, flow data were recorded at pressures of 2, 5, 10, 30, 60, 90, and 100 psid with the downstream pressure at ambient pressure. Primary and repeat flow tests were performed on the $\frac{1}{8}$-in.-diam Carbon-1 and Carbon-2 designs for linear compressions of 0.025 and 0.031 in. (20 and 25% linear compression). For the 0.20-in. diam Carbon-3 and Carbon-4 designs, only primary flow tests were performed at a compression of 0.040 in. (20% linear compression).

During data collection, special care was taken to monitor the relative temperatures of the piston and cylinder. The cylinder outer wall temperature and the inner wall temperature of the hollow piston were monitored. Flow data were only collected when the temperature difference between these surfaces was less than 40°F. Under operating conditions, a 40° temperature difference results in less than a 0.0003 in. change in the sealed gap at 900°F.

A thermal growth differential exists between the carbon-based thermal barrier and the Inconel X-750 superalloy piston. This is

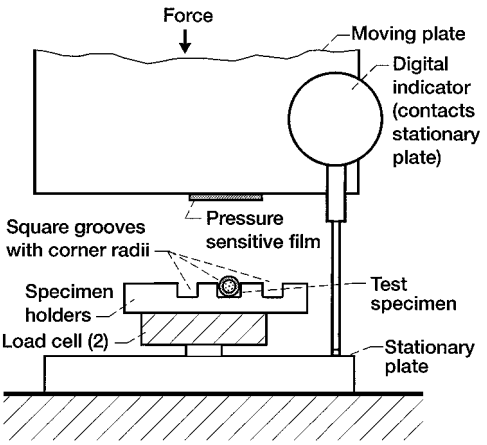

Fig. 4 Schematic of compression fixture.

especially enhanced by the fact that carbon fibers have a negative coefficient of thermal expansion in the longitudinal, e.g., circumferential, direction of −0.3 PPM/°F (Ref. 10). Thus, at high temperatures the piston circumferentially outgrows the thermal barrier, and the specimen ends move apart. To compensate for this phenomenon, the specimen free ends were joined together as a lap joint to prevent a free flow path from forming (Fig. 3). A lap joint of at least $\frac{1}{4}$ in. was used to prevent the joint from opening and to mitigate the effects of 0.053 in. in relative piston-to-thermal barrier differential circumferential growth.

Compression Tests

Compression tests were performed to determine thermal barrier preload and resiliency behavior at room temperature using a precision linear slide compression test fixture shown schematically in Fig. 4. A specimen was loaded into a stationary grooved specimen holder, and an opposing plate was compressed against the specimen. The amount of compressive load on the specimen was measured vs the amount of compression. Thermal barrier compression, or linear crush, was measured using a digital indicator that monitored the movement of the opposing plate relative to the stationary specimen holder. A pressure sensitive film mounted on the opposing plate was used to determine the contact width of the specimen as it was compressively loaded. The film develops under compressive loading so that the specimen leaves a "footprint" after it has been crushed against the opposing plate. The loading characteristics of the pressure sensitive film were described in detail by Steinetz and Adams.[2] Average compressive load, or preload, was calculated by dividing the measured compressive force recorded during loading by the contact area left on the film.

As with the flow tests, stainless steel shims were placed in the groove behind the specimens so that different amounts of linear compression could be examined. The ends of the specimens were lightly glued to prevent the short specimen lengths from unraveling. The specimens used for these tests were $1\frac{1}{2}$ in. in length, and the shims placed behind them were 1 in. long. This allowed the ends of the specimen to hang over the ends of the shims. Isolating the glued ends of the specimens from the test area minimized any possible influence that they could have had on the results.

The procedure that was followed for the compression tests is described in detail by Steinetz et al.[1] This procedure accurately simulates the loading conditions experienced by the thermal barriers in the flow test fixture and allows the preloads under those conditions to be calculated from measured quantities. Multiple load cycles were applied to the specimen before the preload data point was recorded to remove most of the hysteresis and permanent set that accumulates with load cycling of the specimens. Most permanent set occurred within the first four load cycles. The footprint length (nominal 1 in.) and width at the end of the fourth load cycle were used along with the measured load vs compression data to calculate the estimated preload and residual interference corresponding to a given linear crush value.[1] Residual interference is defined as the distance the specimen will spring back while maintaining a load of at least one pound per inch of specimen. The compression cycling procedure also accounts for both the normal and frictional loads that the specimens experience in the flow fixture. This procedure has been validated for the thermal barriers by comparing overhang measurements after a flow test to residual interference measured in the compression tests. The overhang data agreed to within 0.001 in. to that expected from the last cycle compression data.

Compression tests were performed on all four designs of the carbon fiber thermal barrier to determine the specimen preloads corresponding to the linear crushes used in the flow experiments. Tests were performed at compressions of 20, 25, and 30% of each specimen's overall diameter. Primary and repeat compression tests were performed on the Carbon-1 and Carbon-2 designs at linear compressions of 0.025, 0.031, and 0.038 in. The Carbon-3 and Carbon-4 designs were tested at compressions of 0.040, 0.050, and 0.060 in. in both primary and repeat tests.

Subscale Rocket Char Motor Tests

As part of the preliminary feasibility assessment of the thermal barrier, Thiokol Corporation performed tests for NASA using a subscale (70 lbm) rocket char motor. In these tests, the NASA Carbon-5 0.260-in. cross-sectional diameter thermal barrier impeded hot gas flow through an intentional 0.060-in.-deep circumferential defect between rocket case insulation blocks. The insulating blocks were modified to accommodate a $5\frac{1}{8}$ in.-diam thermal barrier. This defect was much larger than any defects that would normally form through the gap-fill material in the actual rocket nozzle joint, but this size was chosen to force gas flow through the thermal barrier under very extreme conditions. Burning solid rocket propellant, the rocket fired for 11 s and generated 900 psi pressures and 5000+ °F (estimated) chamber temperatures. Hot gas flowed to the thermal barrier while upstream and downstream temperatures and pressures were recorded. The char motor incorporated an outboard plenum chamber, or reservoir, to simulate the volume (80 $in.^3$) between the thermal barrier and the Viton O-ring seals. This reservoir ensured that flow would pass through the thermal barrier. The reservoir started at ambient pressure and then quickly reached chamber pressure, simulating the actual RSRM joint fill-time. After the volume between the thermal barrier and Viton O-ring pressurizes in the rocket nozzle joint, charring risk to the Viton O-ring is virtually eliminated.

Results and Discussion

Thermal Barrier Characterization Results

The values for equivalent core diameter, sheath thickness, and overall density are presented in Table 2 for each type of thermal barrier. Of the $\frac{1}{8}$-in. designs, Carbon-1 had the largest core diameter at 0.064 in. and the smallest sheath thickness at 0.025 in. Carbon-2 had a core diameter of 0.038 in. and a sheath thickness of 0.044 in., whereas Carbon-2A had a core diameter of 0.036 in. and a sheath thickness of 0.045 in. The relative proportions of the core and sheath corresponded to the designs of these thermal barriers. All three designs were about $\frac{1}{8}$ in. in diameter, so that Carbon-1 with only five sheath layers had a much larger core than Carbon-2 and Carbon-2A, which had ten and nine sheath layers, respectively. Overall density was inversely related to the number of sheath layers. The design with the most sheath layers, Carbon-2, was the least dense, whereas

Table 2 Equivalent core diameter, sheath thickness, and overall density calculations

Barrier type	Number of sheath layers	Diameter, in.	Equivalent core diameter, in.	Sheath thickness, in.	Overall density, g/cc
Carbon-1	5	0.114	0.064	0.025	1.099
Carbon-2	10	0.125	0.038	0.044	0.998
Carbon-2A	9	0.125	0.036	0.045	1.019
Carbon-3	5	0.200	0.107	0.047	1.035
Carbon-4	5	0.194	0.100	0.047	1.018

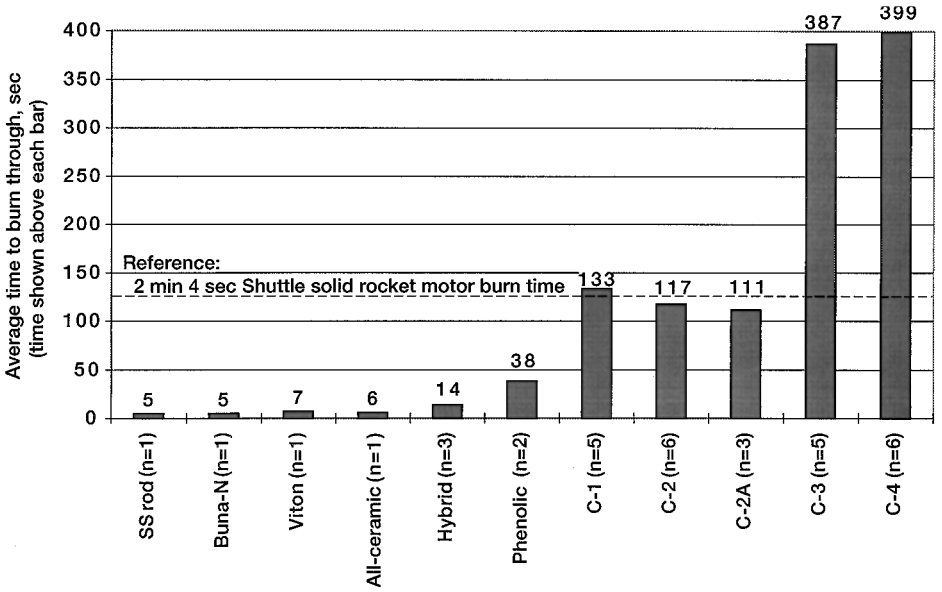

Fig. 5 Oxyacetylene torch burn test results (n = number of tests performed).

the design with the fewest sheath layers, Carbon-1, had the highest density.

The two larger thermal barrier designs, Carbon-3 and Carbon-4, had comparable sheath thicknesses and core diameters. Both had a sheath thickness of 0.047 in., but their core diameters were slightly different at 0.107 in. for Carbon-3 and 0.100 in. for Carbon-4. These values were very similar because both designs had five sheath layers. The overall density for each type of thermal barrier was different though. The Carbon-3 design was more dense than Carbon-4 because of the difference in core fiber sizes. The larger core fibers in Carbon-4 did not pack together as closely as the smaller core fibers in Carbon-3 did. This created more void space in Carbon-4 and lowered its overall density.

Burn Test Results

The amount of time to burn through each type of thermal barrier is shown in Fig. 5. In this figure, the number of specimens that were tested is given under the name of each thermal barrier type, and the average burn-through time is found above each bar. It is obvious from this figure that the carbon fiber thermal barriers are the most burn-resistant type of thermal barrier that was tested. The $\frac{1}{8}$-in. diam designs (Carbon-1, Carbon-2, and Carbon-2A) endured the 5500°F oxyacetylene torch for about 2 min, three times as long as the next nearest design—the phenolic fiber thermal barrier. The larger carbon thermal barriers, Carbon-3 and Carbon-4, were even more impressive, lasting about $6\frac{1}{2}$ min in the flame. This is greater than three times the shuttle solid rocket motor burn time of 2 min, 4 s. After the carbon thermal barriers were removed from the flame, they remained soft and flexible, even in the area that was affected by the flame, with no evidence of fiber melting. All other non–carbon designs lasted less than 15 s, including the $\frac{1}{8}$-in.-diam stainless steel rod that only lasted 5 s. The conventional O-ring materials, Viton (shuttle solid rocket motor seal material) and Buna-N, only lasted 7 and 5 s, respectively. The all-ceramic seals lasted 6 s, although the hybrid seals lasted 14 s. All of the non–carbon designs showed signs of charring or melting after removal from the flame, and many became very brittle in the area that was burned.

Carbon-3 and Carbon-4 with nominal diameters of 0.20 in. lasted about $6\frac{1}{2}$ min in the oxyacetylene torch. In comparison, $\frac{1}{8}$-in.-diam Carbon-1, Carbon-2, and Carbon-2A designs lasted about 2 min. Factors contributing to this threefold increase in burn resistance include an increase in diameter by a factor of 1.6 from $\frac{1}{8}$ to 0.20 in. and an improvement in sheath braid density. Carbon-3 and Carbon-4 were not only larger than Carbon-1 and Carbon-2, but they also had a higher braid angle of 65 deg (nominal) as opposed to 45 deg in the smaller designs. The higher braid angle combined with more braid carriers (12 and 24 carriers for Carbon-3 and Carbon-4 vs 8 carriers for Carbon-1 and Carbon-2) created a more closely packed thermal barrier with a tighter sheath and is believed to have significantly contributed to the greater burn resistance of the larger diameter designs.

As shown in Fig. 5, there was a slight difference in the burn resistance of Carbon-3 and Carbon-4. Carbon-3 lasted an average of 387 s (6 min 27 s) in the flame, while Carbon-4 lasted an average of 399 s (6 min 39 s). This difference of only 12 s over a 6–7 min test is most likely not significant in that it is only a 3% difference in time to burn through the specimens. However, it is possible that the larger diameter pitch fibers in the core of Carbon-4 (see Table 1) provided a very small improvement in the burn resistance of this design over the Carbon-3 design that had smaller PAN-based fibers in its core.

Mass-Loss Mechanism

The mass-loss mechanism for the carbon thermal barriers is believed to be carbon oxidation. Depending on material type, carbon fibers begin to oxidize at temperatures in the range of 600–900°F (Refs. 5–7). Mass loss is not because of carbon sublimation because this process occurs at 6900°F (Ref. 11), significantly above the 5500°F flame temperature. Further evidence that the mass-loss mechanism is primarily oxidation is that when adjusting the flame from neutral (as described herein) to heavily oxidizing, burn-through times for Carbon-1 and Carbon-2 thermal barriers were only 8% of those reported in Fig. 5.

Products of combustion in the solid rocket motor include liquid alumina (Al_2O_3) and gaseous CO, ClO_2, Cl, HCl, and H_2, none of which are oxidative. Hence, it is believed that the neutral flame in ambient air (oxidizing) is a conservative, i.e., more aggressive, environment for performing material screening burn tests. It is expected that oxidation rates within the rocket environment will be slower than those exhibited herein.

Flow Test Results

Flow rates for the four carbon thermal barrier designs at different levels of linear compression are summarized in Fig. 6 at 60 psi and 70, 500, and 900°F after scrubbing. Results for Carbon-1 and Carbon-2 are an average for two tests, whereas those for Carbon-3 and Carbon-4 are for one test only. As shown by the flow results for Carbon-1 and Carbon-2, flow resistance increased with higher compression levels. Figure 7 presents flow vs pressure data for the 0.20-in.-diam Carbon-3 design at a linear compression of 0.040 in. (20%) at pressures of 2–100 psid and temperatures of 70, 500, and 900°F.

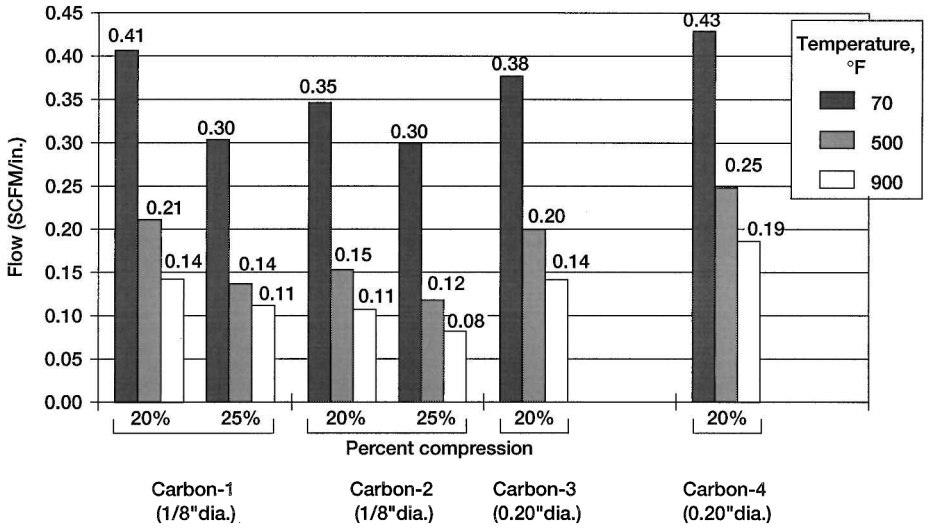

Fig. 6 The effect of temperature, thermal barrier type, and compression on flow after scrubbing, $\Delta P = 60$ psi.

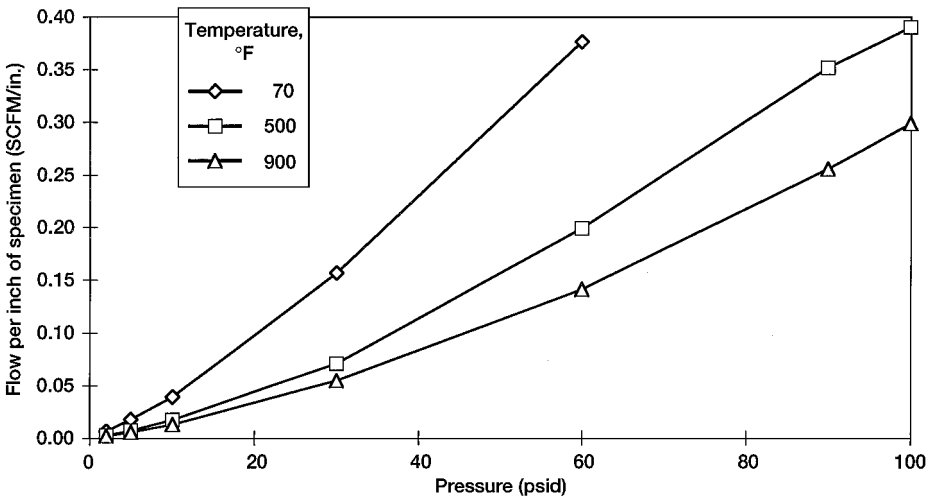

Fig. 7 Flow vs pressure data for three temperatures, 0.20-in.-diam Carbon-3, 0.04-in. (20%) linear compression, after scrubbing.

The flow through this thermal barrier is high enough to permit a leak check of the primary and secondary O-rings without false-positives. Primary sealing of the nozzle joints would still be the responsibility of the O-rings, so that enough flow must pass through the thermal barrier so as not to qualify mistakenly for use a damaged or nonworking O-ring. Figure 7 is representative of the flow vs pressure curves recorded for the other carbon thermal barriers. It shows that the flow rate at each temperature was approximately a linear function of pressure. Additionally, both Figs. 6 and 7 show that flow rates dropped for each thermal barrier as the temperature was increased. This phenomenon is explained by the relationship that gas viscosity increases with temperature, $\mu \propto T^{2/3}$. Thus, as the viscosity of the gas flowing past the thermal barriers increased, the flow rate decreased. This decrease in flow rate through braided rope seals as temperature increases was observed previously by Steinetz and Adams.[2]

Effect of Core Fiber Diameter

Core fiber diameter also affected flow rates. As shown in Table 1, the core fibers in Carbon-3 had a diameter of 2.76×10^{-4} in. (6.9 μm), whereas those in Carbon-4 were 4.4×10^{-4} in. (11 μm). The flow rates given in Fig. 6 for Carbon-4 are about 20% greater than those for Carbon-3. Because the larger core fibers in Carbon-4 did not pack together as closely as the smaller core fibers in Carbon-3 did, larger gaps and flow paths formed through the core of Carbon-4 thermal barriers.

Effect of Hot Scrubbing

No major scrubbing-induced damage was observed on any of the carbon thermal barriers at the conclusion of the flow tests. Any damage that was seen was concentrated immediately around the lap joints and was characterized mainly by fraying of the specimen ends. Figure 8a shows a close-up view of a Carbon-1 specimen tested at 0.025 in. (20%) linear compression after 10 scrub cycles. Some minor damage can be observed around the lap joint. Figure 8b shows a close-up view of a Carbon-4 thermal barrier tested at 0.040 in. (20%) linear compression after 10 scrub cycles. Again, only minor damage can be seen at the lap joint. Minor fraying of the sheath fibers was rarely seen in other areas of the specimens.

Carbon thermal barrier flow rates typically rose after hot scrubbing during flow tests. After 500°F testing Carbon-1 and Carbon-2 flow rates rose as much as 30% and Carbon-3 and Carbon-4 flows rose less than 10%, as compared to the flow rates before scrubbing. Postscrub room temperature flows for all thermal barriers were done after time spent at 500°F (2 h) and 900°F (1.5 h). Postscrub room temperature flow rates for Carbon-1 and Carbon-2 doubled and those for Carbon-3 and Carbon-4 rose 80%, as compared to their prescrub values. It is believed that much of the flow rate increase is because of oxidation that occurred while the specimen soaked at these high temperatures. A simple test was performed to test this hypothesis in which short lengths of carbon thermal barrier were heated in

Table 3 Carbon fiber thermal barrier contact width, preload, and residual interference for several linear crush conditions

Barrier type	Diameter, in.	Nom. percent linear crush, %	Linear crush, in.	Number of sheath layers	Contact width, in.	Preload, psi	Residual interference,[a] in.
Carbon-1	0.114	20	0.025	5	0.038	430	0.012
		25	0.031		0.052	770	0.015
		30	0.038		0.062	1300	0.019
Carbon-2	0.125	20	0.025	10	0.039	380	0.013
		25	0.031		0.055	465	0.019
		30	0.038		0.065	740	0.023
Carbon-3	0.200	20	0.040	5	0.063	310	0.019
		25	0.050		0.082	490	0.027
		30	0.060		0.099	930	0.033
Carbon-4	0.194	20	0.040	5	0.052	430	0.019
		25	0.050		0.077	490	0.028
		30	0.060		0.100	800	0.035

[a]Residual interference is defined as the distance that the thermal barrier will spring back while maintaining a load of at least one pound per inch of specimen.

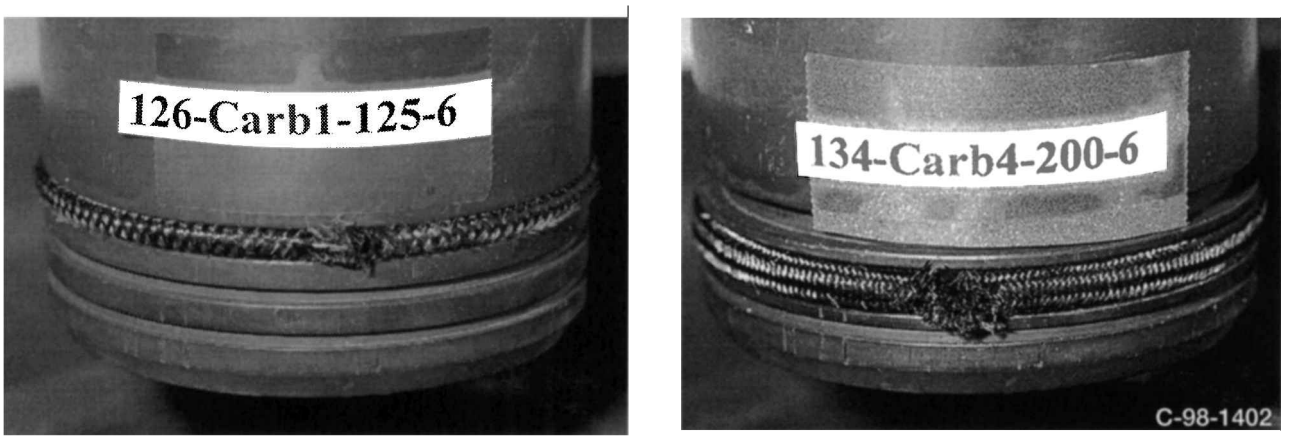

a) Carbon-1 (0.125 in. diam) **b) Carbon-4 (0.20 in. diam)**

Fig. 8 Photos of carbon thermal barriers after 900°F flow/scrubbing tests.

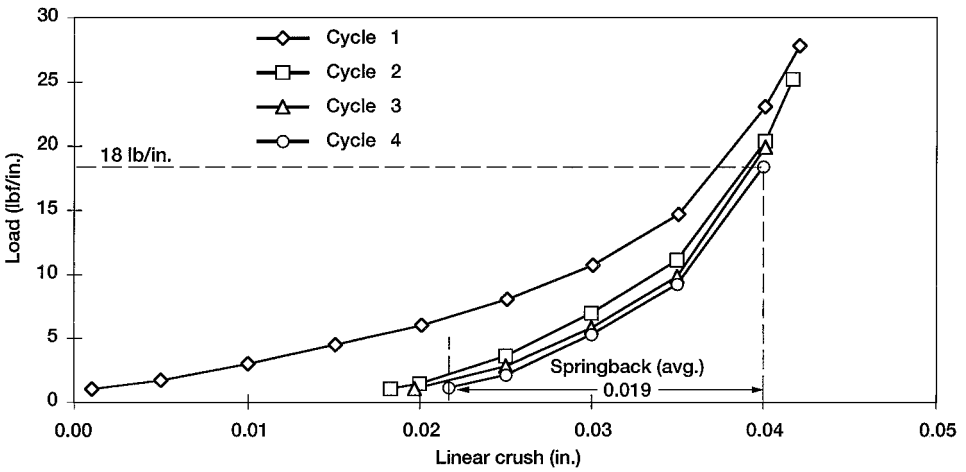

Fig. 9 Load vs linear compression data for four cycles, 0.20-in.-dim Carbon-3 thermal barrier at representative compression of 0.04 in. (20%).

a furnance at different temperatures for 2-h exposures. Specimen weights were measured before and after exposure to the furnance. Results of this test showed that a weight loss of only 1% occurred after 2 h at 500°F, but a 33% weight loss occurred after 2 h at 900°F. Clearly the carbon thermal barriers oxidized when exposed to temperatures of 900°F for extended periods of time, and the associated weight loss that took place contributed to the increased flow rates after scrubbing.

Compression Test Results

Table 3 summarizes the results of the compression tests performed on all four carbon thermal barrier designs. Values listed in this table include the measured contact width, preload, and residual interference for each amount of linear compression, or crush, at which the tests were performed. Figure 9 shows the load vs displacement characteristics for the 0.20-in.-diam Carbon-3 design for a linear crush of 0.040 in. (20% linear compression). This figure is typical of the type of data that is recorded from a compression test on the carbon thermal barriers. It shows that the load vs displacement curves for each load cycle converge as the number of cycles increases.

Contact Width

As shown in Table 3 the contact width increased for every thermal barrier design as the amount of linear crush was increased. This

shows that the carbon thermal barriers continued to spread and flatten out as they experienced larger amounts of compression. In each test, the footprint pattern left on the pressure sensitive film after a compression cycle was solid and continuous. This indicates that during a flow test continuous contact is made between the walls of the flow fixture and the thermal barrier, minimizing leakage past the specimen. No major differences in contact width were seen between the two $\frac{1}{8}$-in.-diam designs, Carbon-1 and Carbon-2. However, the contact widths of the two larger designs did exhibit some differences. At 0.040 and 0.050 in. of linear compression, Carbon-3 had larger contact widths than Carbon-4. This was probably because of the greater ability of the smaller core fibers in Carbon-3 to move past each other and spread out as compared to the larger core fibers in Carbon-4. These differences were minimized at 0.060 in. of compression, though, as the contact widths of the two designs were almost identical. As expected, contact width increased as specimen diameter increased from 1.25 to 0.20 in.

Preload

The amount of preload also increased as the amount of linear crush increased for each type of carbon thermal barrier. Although no differences were found in the contact widths of Carbon-1 and Carbon-2, there were rather significant differences in the preloads of these two designs, as shown in Table 3. For each compression level, the preload for Carbon-1 was larger than for Carbon-2, and the difference between the two designs increased as the amount of linear crush increased. Thus, Carbon-1 specimens were stiffer than Carbon-2 specimens. The reason for this difference is believed to be related to the architecture of the two designs as shown in Table 1. Carbon-2 had 10 sheath layers and a much smaller core area than Carbon-1, which only had 5 sheath layers. In a tightly packed core of uniaxial fibers, there is little room for individual fibers to move with respect to one another when they are compressed. In contrast, fibers in the sheath are oriented at an angle with each other and are better able to slide past each other when the specimen is compressed. Because Carbon-2 had a larger percentage of its total volume in the sheath as compared to Carbon-1, the Carbon-2 design was more easily compressed and had lower preload values.

Carbon-3 and Carbon-4 did not exhibit the same type of behavior in terms of preload as the smaller seals did. Carbon-4 was stiffer at the lowest crush level (0.040 in.), whereas Carbon-3 was stiffer at the highest crush level (0.060 in.). Both designs had the same preload at 0.050 in. of linear compression. The difference in preload behavior is again probably related to the difference in core fibers between the two designs. These larger designs were generally stiffer than Carbon-2 but were still not as stiff as Carbon-1.

Residual Interference

As with the contact width and preload, the residual interference also increased for each type of thermal barrier as percent linear crush increased. Carbon-2 consistently had higher residual interference values at each level of linear crush than Carbon-1 had. Because Carbon-1 was stiffer than Carbon-2, the higher preloads on Carbon-1 caused it to experience larger amounts of permanent set and to lose resilience. Thus, Carbon-1 had less springback in it which led to lower residual interference values. For the larger thermal barrier designs, the residual interference of Carbon-3 and Carbon-4 was almost identical for each amount of linear compression. Residual interference for Carbon-3 and Carbon-4 was 0.019 in. even for the lowest compression (20%) and meets the design requirement to follow nozzle joint movement/separation (0.003–0.005 in.) during shuttle solid rocket motor operation. Table 3 also shows that residual interference scaled approximately with diameter. When specimen diameter was increased by a factor of 1.6 from 0.125 to 0.200 in., residual interference was also increased by that ratio for each level of percent compression.

Results of Thiokol Char Motor Tests on Carbon Thermal Barriers

Thiokol tested a 0.260-in.-diam thermal barrier for NASA in a subscale rocket motor to verify that it would withstand the shuttle solid rocket motor environment. The subscale motor, or char motor, simulates the thermal conditions of the full-scale motor by burning solid rocket propellant at corresponding chamber pressure and temperature conditions. The thermal barrier was placed into an intentional gap defect between the phenolic insulating blocks, as shown in Fig. 10a. The combination of an outboard plenum chamber and the 0.060-in. circumferential gap extending both upstream and downstream of the thermal barrier ensured that hot gas flow would pass through the thermal barrier. Temperatures and pressures were measured both upstream and downstream of the thermal barrier during testing.

Throughout the test duration of approximately 11 s, a significant drop in temperature was measured across the thermal barrier. Figure 10b shows that the maximum temperature seen on the hot side of the barrier was over 3200°F, whereas the cold side temperature reached about 950°F. A temperature drop of about 2200°F occurred across the $\frac{1}{4}$-in.-diam thermal barrier. Another finding from this test was that although the rocket core temperatures can reach 5500°F, significant cooling of the gases occurs in the boundary layer and in the small gaps leading to the thermal barrier thereby reducing the incoming gas temperature to 3200°F. Pressure readings upstream and downstream of the thermal barrier and in the reservoir indicated that there was gas flow across the thermal barrier. Just as importantly, there was no apparent burning or charring of the thermal barrier on inspection after removal from the motor.

Although the 950°F temperature recorded downstream of the thermal barrier is still higher than the temperature limits of the Viton nozzle O-rings, the thermal barrier caused a 2200°F temperature drop in the incoming gas. In addition, the thermal barrier diffused the focused nature of the hot gas jet, further reducing the jet's potentially damaging effects on downstream Viton O-rings in the actual shuttle solid rocket motor. The char motor subjected the thermal barrier to more aggressive conditions than would ever occur

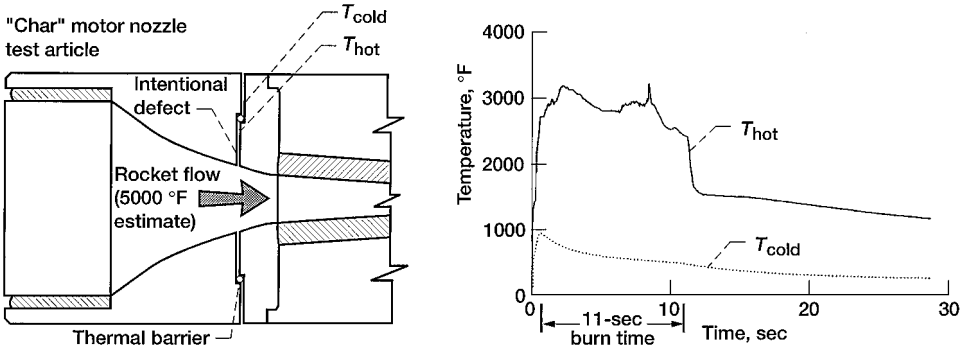

a) Test configuration: Carbon-5 thermal barrier impedes hot gas flow through intentional joint defect (0.06 in. gap)

b) Temperature data: Upstream (T_{hot}) and downstream (T_{cold}) sides of thermal barrier. (Courtesy of Thiokol Corp.)

Fig. 10 Preliminary subscale (70 lbm) char motor tests examining thermal barrier (Carbon-5) effectiveness.

in the actual shuttle solid rocket motor for the following reasons. As stated previously, the gap defect was purposely oversized at 0.060 in. to force flow through the thermal barrier. In the actual nozzle joint, the gap between adjoining blocks of insulation would be much narrower as the pieces of insulation are basically in contact with each other. The narrow gaps between the phenolic insulation would significantly cool the incoming gas temperature impinging on the thermal barrier and would therefore lower the temperature of the gas that reaches the Viton O-rings. Furthermore, the downstream temperature in the char motor test was recorded immediately downstream of the thermal barrier. The O-rings in the rocket nozzle joint are located several inches further downstream of the thermal barrier, allowing additional heat to be removed from gas jets that flow through the thermal barrier before they reach the O-rings.

Conclusions

The 5500°F combustion gases in the shuttle solid rocket motors are kept a safe distance away from the seals in assembly joints by thick layers of phenolic insulation and by special compounds that fill assembly split-lines in this insulation. Parasitic leakage paths have occasionally opened up in the gap-filling compounds and allowed a direct flowpath of hot gases to the seals causing O-ring seal erosion and charring. NASA and solid rocket motor manufacturer Thiokol are investigating the feasibility of using NASA braided thermal barriers upstream of the primary O-rings. These thermal barriers would resist the hot gases and prevent them from reaching the primary O-rings.

The thermal resistance of different material systems was assessed by exposing thermal barriers to an oxyacetylene torch at 5500°F (representative of solid rocket motor combustion temperatures) and measuring time for burn-through. Thermal barriers braided out of carbon fibers exhibited the longest time for burn-through. Flow and durability tests were conducted on the carbon thermal barriers to examine their leakage characteristics and durability at ambient and high temperatures. Room temperature compression tests were performed to determine load vs linear compression, preload, contact area, and residual interference/resiliency characteristics. Subscale rocket char motor tests were performed in which hot combustion gases were allowed to flow to the thermal barrier to assess its thermal resistance in a rocket environment. Based on the results of these tests, the following conclusions are made.

1) Carbon-3 and Carbon-4 springback of 0.019 in. is greater than the 0.003–0.005 in. joint movement/separation anticipated during rocket motor operation, providing adequate resiliency.

2) Carbon-3 and Carbon-4 thermal barriers resisted the oxyacetylene flame (5500°F) for over 6 min before burn-through, greater than three times shuttle solid rocket motor burn time.

3) Subscale rocket char motor tests successfully demonstrated that the thermal barrier resisted hot gases that flowed to it through an intentionally oversized gap defect. A 2200°F temperature drop was observed across the $\frac{1}{4}$-in.-diam thermal barrier during the 11-s rocket firing.

4) Laboratory flow, compression, burn tests, and subscale rocket char motor tests demonstrate the thermal barrier's preliminary feasibility, qualifying the thermal barrier for comprehensive test and evaluation.

Acknowledgments

The authors gratefully acknowledge Doug Frost's and Peter Totman's (Thiokol) thermal barrier char motor test results; Bruce Bond's (Albany-Techniweave) assistance in fabricating the thermal barriers, and Tom Doeberling's (NASA) assistance in test support.

References

[1]Steinetz, B. M., Adams, M. L., Bartolotta, P. A., Darolia, R., and Olsen, A., "High Temperature Braided Rope Seals for Static Sealing Applications," NASA TM-107233 rev., July 1996, also *Journal of Propulsion and Power*, Vol. 13, No. 5, 1997, pp. 675–682.

[2]Steinetz, B. M., and Adams, M. L., "Effects of Compression, Staging, and Braid Angle on Braided Rope Seal Performance," NASA TM-107504, July 1997.

[3]Scott, R. S., "RSRM-45A Nozzle Joint No. 3 O-Ring Erosion Investigation Team Final Report," Thiokol Rept. TWR-73191, Brigham, UT, Oct. 1996.

[4]Shemet, V., Pomytkin, A. P., and Neshpor, V. S., "High-Temperature Oxidation Behavior of Carbon Materials in Air," *Carbon*, Vol. 31, No. 1, 1993, pp. 1–6.

[5]Bahl, O. P., and Dhami, T. L., "Oxidation Resistance of Carbon Fibers," *High Temperatures-High Pressures*, Vol. 19, No. 2, 1987, pp. 211–214.

[6]Eckstein, B. H., and Barr, J. B., "An Accelerated Oxidation Test for Oxidation Resistant Carbon Fibers," *Materials-Processes: The Intercept Point; Proceedings of the Twentieth International SAMPE Technical Conference*, Society for the Advancement of Materials and Process Engineering, Covina, CA, 1988, pp. 379–391 (Minneapolis, MN, Sept. 1988).

[7]Eckstein, B. H., "The Weight Loss of Carbon Fibers in Circulating Air," *Proceedings of the 18th International SAMPE Technical Conference*, Society for the Advancement of Materials and Process Engineering, Covina, CA, 1986, pp. 149–160 (Seattle, WA, Oct. 1986).

[8]Ballis, W., *ASM Handbook, Volume 6: Welding, Brazing, and Soldering*, ASM International, Materials Park, OH, 1993, pp. 281–290.

[9]Udin, H., Funk, E. R., and Wulff, J., *Welding for Engineers*, Wiley, New York, 1954, pp. 211–218.

[10]Thornel T-300 carbon fiber Product Information, Amoco Performance Products, Inc., Alpharetta, GA, March 1994.

[11]Lide, D. R., and Kehiaian, H. V., *CRC Handbook of Thermophysical and Thermochemical Data*, CRC Press, Boca Raton, FL, 1994, pp. 25–31.